Stability Optimization of Two-Fingered Anthropomorphic Hands for Precision Grasping with a Single Actuator

Michael T. Leddy, *Student Member, IEEE* and Aaron M. Dollar, *Senior Member, IEEE*

Abstract— In this paper, we present a constrained optimization framework for evaluating the post-contact stability of underactuated precision grasping configurations with a single degree of actuation. Relationships between key anthropomorphic design parameters including link length ratios, transmission ratios, joint stiffness ratios and palm width are developed with applications in upper limb prosthetic design. In addition to grasp stability, we examine post-contact system work, to reduce reconfiguration, and consider the range of objects that can be stably grasped. External wrenches were simulated on a subset of the heuristically evaluated optimal solutions and an optimal configuration was experimentally tested to determine favorable wrench resistible gripper orientations for grasp planning applications.

I. INTRODUCTION

Underactuated mechanical systems with significantly more degrees of freedom than actuators have been utilized in the field of robotic grasping to provide a grasp that is adaptive and robust without the need for complex control. This approach is extensively applied in the field of upper limb prosthetics [1-4] in which nominally ten to fifteen degrees of freedom are controlled by only a few actuators using coupling mechanisms in the palm and fingers. The compliance in these mechanisms facilitate multiple points of contact during enveloping grasps that can accommodate the arbitrary object positioning, orientation and size seen in unstructured environments [5][6]. However, in a two-fingered precision grasp, which is generally necessary to grasp small objects, unconstrained degrees of freedom and decreased force production from passive elastic elements provide potential reconfiguration and instability. An ideal underactuated hand should combine both wrap grasp performance with precision grasps stability to be effective for a variety of objects.

To ensure that the precision grasp of an object remains stable, the hand-object system must remain stable at contact and as it reconfigures. To determine stability, concepts such as force closure and the equilibrium point may be examined. Finger stability occurs in underactuated two link fingers when the equilibrium point, the location in which the contact, actuation and interlink force lines of action intersect, is within the friction cone [7]. An object is considered to be stable in precision grasp when it satisfies force closure, indicating the forces applied between antipodal contact points on an object are positive or zero, the contact line lies within each friction cone and net wrench on the object is zero [8].
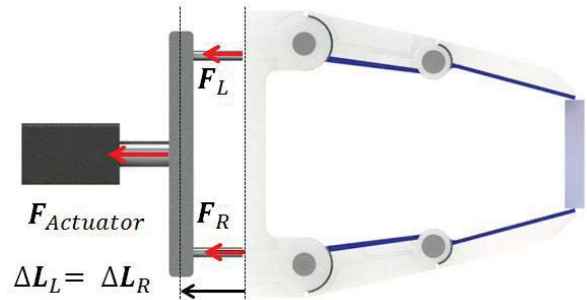
Figure 1.   A two-fingered underactuated tendon driven hand model precision grasping an object with a single actuator in force control.

Recent research has taken many different approaches to address the stability issue seen in underactuated precision grasping. In [9], the equilibrium point was investigated to develop mechanical joint limits and determine optimal contact locations for a single actuator grasper with a force differential. On-contact stability was further investigated in a finger that could manipulate its static equilibrium point by mechanically changing its transmission ratio [10]. A constrained optimization was implemented to determine finger parameters for successful form closure of a single actuator multi-link robotic gripper [11] and to determine the passive wrench resistibility of a two-fingered hand fixed in force control [12]. Stable reconfiguration has been investigated for controlled manipulation of two separately actuated, underactuated fingers [13] and for the motion compensation of a similar underactuated gripper [14]. Although stability has been investigated in two finger precision grasping, minimal research addresses the optimality of these configurations for grasping where sophisticated control of the end effector is not possible due to limited number of actuators nominally controlled open loop.

In this paper, we present a multi-step constrained optimization framework for evaluating grasp stability including the post contact reconfiguration and the wrench resistibility of two-fingered precision grasping configurations in which parameters are sampled in anthropomorphic configurations. The optimization platform is modeled off of the kinematics of tendon-driven underactuated hands that are driven from a single actuator. To determine optimal solutions, additional criteria were evaluated including a minimization of post-contact work, to reduce reconfiguration, and maximize the stable object size (Fig. 2A,2B). Maximally performing configurations were simulated and one configuration was experimentally tested to determine favorable wrench resistible gripper orientations for grasp planning applications (Fig. 2C). Relationships between key anthropomorphic design parameters were developed and

interpreted for implications in robotic end effectors and upper limb prosthetic design.

II. METHODS

A. Stability and Contact Model

When defining stability of the hand-object system in precision grasp, we determined that both the finger and object should be in quasistatic equilibrium at contact and while reconfiguring. The underactuated hand was modeled as two symmetric two-link fingers grasping orthogonal rectangular objects in point contact with coulomb friction (Fig 3.), where contact force (F_c) can be applied at any direction with the friction cone angle $\alpha = arctan(\mu)$. Force closure determined object stability in this model, requiring the forces applied between antipodal contact points on an object to be positive or zero, the contact line to lie within each friction cone and the net wrench on the object is zero. However, the antipodal grasp theorem tells us that the object will remain stable with our contact model. As an additional heuristic, the equilibrium point (P_{EQ}) location relative to the friction cone, was introduced to evaluate the quality of grasp stability for a given grasp. When the equilibrium point is within the friction cone there exists a wrench that the finger can exert without slipping or reconfiguring to stabilize the object [7]. We described this equilibrium point configuration as a reliable precision grasp and implemented grasp reliability as an additional criteria for evaluating finger stability under arbitrary external disturbances.

Failure to stabilize the object was determined when force closure of the object was broken or finger equilibrium was not ensured with the grasp reliability heuristic. This was simplified into four main stability criteria for each finger. First, the tendon force magnitude (F_T) being positive or zero, the contact force magnitude $\|F_c\|$ being positive or zero, the contact force vector ($\vec{F}_c$) between antipodal points is located in the friction cone manifold given object tilt (θ_{ob}) and the finger contact force vector and contact moment arm (F_c, R_c), interlink force vector and moment arm (F_l, R_l), and tendon force vector and moment (F_T,R_T) are in force and torque equilibrium. It is noted that under external wrenches the contact force vector and antipodal line are not collinear, when the contact force vector points outside of the friction cones the object experiences slip. When these criteria, listed below, are satisfied the hand-object system reconfigures like a constrained six bar mechanism.

$$F_{TL} \geq 0 \quad , \quad \|F_C\| \geq 0 \tag{1}$$

$$\mu - \tan(\theta_{obj}) \leq \frac{|F_{cy}|}{|F_{cx}|} \leq \mu + \tan(\theta_{obj}) \tag{2}$$

$$\sum \vec{r}_i \, x \, \vec{F}_i = 0 \tag{3}$$

B. Parameter Reduction and Constraints

Constraints were placed on feasible parameters to reduce the sample space of the optimization. Configurations were normalized and sampling ranges were limited to reflect that of anthropomorphic configurations that were kinematically feasible. Anthropomorphism was preferred for the underactuated hand parameters because these configurations nominally produce favorable wrap grasp performance [7] and we aimed to retain these benefits as we further optimized the precision grasping performance. The initial sampled parameters were simplified to three normalized independent variables, the distal radius (r_d), the distal link length (L_d), and the palm width L_{palm}. The proximal finger length (L_p) was determined by keeping the total finger length constant such that $L_p = 1 - L_d$. The value for the proximal radius r_p was kept consistent to determine the transmission ratio and the proximal joint stiffness (K_p) was kept consistent to determine the distal stiffness (K_d) given a predetermined anthropomorphic free swing trajectory constant (c_{fs}) that maps the relative movement of the finger proximal joint (θ_p) and distal joint (θ_d) in free swing.

$$c_{fs} = \frac{r_d}{r_p} \frac{K_p}{K_d} \tag{4}$$

The post-contact reconfiguration of the system from increased actuator force or external disturbances was modeled as a constrained six bar mechanism. The system kinematics were evenly constrained to regularize the optimization. This produced a unique solution for each of the eleven variables that kinematically determined our model. Variables included are the proximal and distal joint angle for the left and right fingers (θ_1, θ_2 and θ_3, θ_4), the object tilt (θ_{ob}), the left and right tendon forces (F_{TL}, F_{TR}) and the X and Y components of the contact force for the left
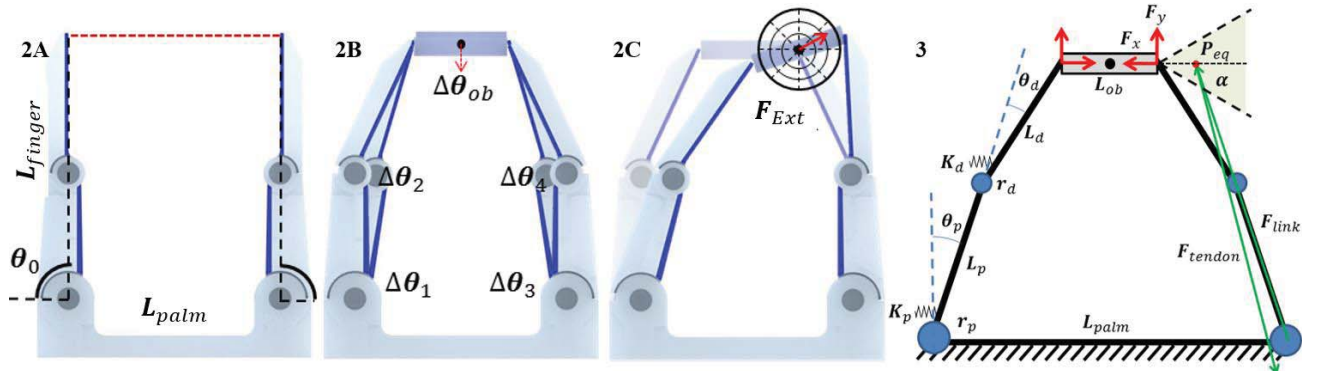
Figure 2. The process for evaluating stability for two-fingered precision grasping including (a) the starting position of the hand and (b) a constrained optimization of the six bar mechanism to determine reconfiguration and (c) evaluating the stability of configurations to external wrenches .
Figure 3.   A kinematic model of the two fingered system describing the starting positions, design parameters, kinematics and contact model.

and right finger (F_{XL}, F_{YL} and F_{XR}, F_{YR}). First, the tendon tension must balance the actuator force (F_{act}) so that the fingers remain in equilibrium with the actuator. Coupled tendons also inferred that the tendon length change in the fingers (ΔL_{TL}, ΔL_{TR}) must be equal. The next two constraints, evaluated at an initial configuration (θ_0), required that the six bar linkage closure constraints were unviolated to ensure object contact was maintained throughout the grasp.

$$F_{act} = F_{TL} + F_{TR} \tag{5}$$

$$r_1\theta_1 + r_2\theta_2 = r_3\theta_3 + r_4\theta_4 \tag{6}$$

$$\begin{bmatrix} L_1c_1 + L_2c_{12} \\ L_1s_1 + L_2s_{12} \end{bmatrix} + \begin{bmatrix} L_{ob}c_{ob} \\ L_{ob}s_{ob} \end{bmatrix} = \begin{bmatrix} L_3c_3 + L_4c_{34} + L_{palm} \\ L_3s_3 + L_4s_{34} \end{bmatrix} \tag{7}$$

Where s_{12} and c_{34} are shorthand for $\sin(\theta_1 + \theta_2)$ and $\cos(\theta_3 + \theta_4)$ and angles are evaluated in the direction of closure. The finger torque balance provides four equations and ensures both fingers are in static equilibrium while grasping the object. In this formulation, the actuator torque must equal the elastic element restoring torque plus the contact torque. The product between the actuator jacobian, describing the actuation lever arms $J_{act}^T = [r_1 \ r_2 \ r_3 \ r_4]$, and the tendon force ($F_{act}$), consisting of F_{TL} and F_{TR}, produces the actuator torque. The product of diagonalized spring stiffness (K_{1-4}) and the net closure $\Delta\theta_{1-4}$ produces the spring restoring torque. Last, the product of the contact jacobian, mapping the moment arms of the joints to the contact point, $J_c^T(\theta_i, \theta_{ob})$, and the contact forces $F_c = [F_{XL} \ F_{YL} \ F_{XR} \ F_{YR}]$ produces the contact torque. The last three constraint equations are generated from the object static equilibrium conditions that must balance an applied external wrench. In this constraint which F_c is the concatenated contact force vector for each finger, G is the grasp matrix that maps the contact forces to the object frame and $\vec{F}_{ext}$ is the external wrench. The contact jacobian $J_c^T(\theta_i, \theta_{ob})$ and grasp matrix G form are explained in further detail in [13].

$$J_{act}^T F_{act} = K_i \Delta\theta_i + J_c^T(\theta_i, \theta_{ob}) F_c \tag{8}$$

$$G F_c + F_{ext} = 0 \tag{9}$$

Constraints and failure criteria were considered in every step of the constrained optimization. Configurations that violated the constraints or failure criteria were eliminated during each step of the parameter search. The initial set of stable solutions were configurations that remained stable at contact and during reconfiguration up to a determined maximum tendon force (F_{Tmax}) for objects from 0% to 50% of the finger length. These percentages were chosen to represent precision grasping of a variety of small to large objects. The configurations that passed this initial stability heuristic were passed through two additional criteria to evaluate their performance for practical robotic grasping focused on reliably grasping a large variety of object sizes and reducing post-contact work.

C. Evaluating Optimal Configurations

Two additional criteria were established to evaluate stable configurations for favorable performance in grasping tasks. Due to instability in two-fingered underactuated precision grasping from slipping or ejection [15], one is usually limited to grasping a small variety of objects. This is partly attributed to reconfiguration that can occur in underactuated hands post-contact requiring compensatory movement to adequately place an object [14]. Thus, favorable designs of underactuated hands include the ability to stably grasp a variety of object sizes with minimal system reconfiguration.

The first objective was to find configurations that produce the maximum reliable object size which we defined as L_{objmax} normalized to the finger length. This was calculated using the previous constrained optimization and varying L_{obj} > 50% finger length until failure. The second objective was to minimize post-contact work of the hand-object system to reduce post-contact joint motion and object reconfiguration. Post-contact work (ΔW_{pc}) was calculated as the integral of product of the post-contact change in tendon force, $F_{Tpc} = F_{Tmax} - F_{Ti}$, and the difference in tendon length $\Delta L_{Tpc} = L_{Tf} - L_{Ti}$. Where F_{Tmax} is the maximum actuator force, F_{Ti} is the tendon force at contact, L_{Tf} is the tendon length after reconfiguration and L_{Ti} is the tendon length at contact. Minimizing this metric reduces the amount of compensation a robotic system may have to do to account for this motion.

$$\Delta W_{pc} = \int F_{Tpc} \Delta L_{Tpc} \tag{10}$$

To evaluate configuration performance, an optimization function was incorporated to produce a weighted score of the given configuration combining the stable grasp width and post-contact work. This weighted score (C_{score}) is a maximization of the three elements, the post-contact work for a very small object $S_1 = 1/\Delta W_{pc0\%}$, the post-contact work for a large object $S_2 = 1/\Delta W_{pc50\%}$, and the normalized maximum reliable grasp span $S_3 = L_{objmax}/L_{finger}$. The constant A_i determines the weight of each element in the optimization function. Each individual value is normalized against the maximum and minimum range of values in the stable configuration solution space to eliminate bias in the case elements have different variability.

$$C_{score} = \sum A_i \frac{S_i - \min(S_i)}{\max(S_i) - \min(S_i)} \tag{11}$$

D. External Disturbance Analysis

Once weighted values were determined, an external wrench was applied to the already grasped object for the top 40% of maximally performing configurations to determine configuration stability. The external disturbance was applied in the global frame and acted in the center of the grasped object to determine the maximum resistible wrench, a measure of configuration post-contact stability [16]. This metric also further evaluates the stability of fringe cases where the maximally performing solutions fall close to the stability solution hull. External disturbances can create force asymmetry which removes the mirrored motion of the

TABLE I.   SIMULATION RESULTS

Parameter	Stable Reconfiguration (0% to 50% L_f)				
	Min	Mean	Max	Range	Tested
Link Length Ratio (L_d/L_p)	0.680	1.085	1.460	[0.68-1.46]	1.403
Transmission Ratio (R_d/R_p)	0.383	0.503	0.583	[0.01-1]	0.583
Stiffness Ratio (K_d/K_p)	0.548	0.719	0.833	[0.01- ∞]	0.833
Palm Width (L_{palm}/L_{finger})	0.500	0.945	1.500	[0.5-1.5]	0.770
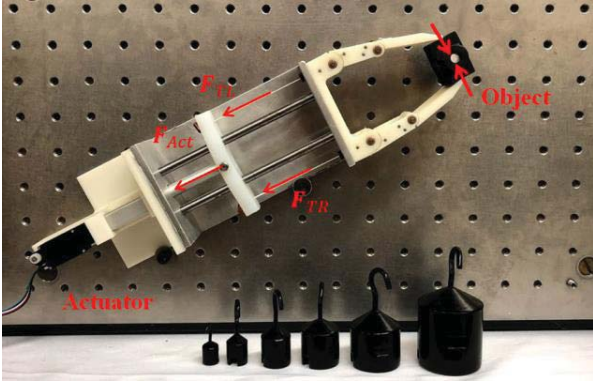
Figure 4. Experimental test setup including a linear actuator, coupled tendons, a hand and object. Weights were applied to the center of the object with gravity applying a force in the global frame.

proximal and distal joints (θ_p, θ_d), allowing nonzero object tilt (θ_{ob}) and differences in tendon force (F_{TL}, F_{TR}). For simplicity the system can be modeled as an asymmetric constrained six bar linkage, subject to elastic elements and joint limits, to solve for displacement of hand-object system.

To experimentally test and validate the simulation a two-fingered precision grasper was developed using parameters from a sample optimal solution seen in Fig. 4. A single linear actuator drove two symmetric fingers in open loop force control. The 30 gram object was acquired and the actuator tendon was tensioned to a designated force allowing the system to reconfigure. To simulate an external disturbance in the global frame, the apparatus was placed in a variety of orientations and weights were slowly added to the center of the object until object slip occurred. The maximum resistible wrench and external disturbance profile was calculated and compared to the simulation results.

III. RESULTS AND DISCUSSION

A. Precision Grasp Stability

A parameter search of three independent variables (r_d, L_d, L_{palm}), bounded by initial sampling constraints on anthropomorphism and kinematic feasibility, was conducted to determine stable configurations using gradient descent of a constrained nonlinear multivariable function in MatLab [17]. The free swing trajectory constant (c_{fs}) was set to 0.7 to resemble an anthropomorphic hand [18] with a large grasp envelope. Given our initial model, 0.1% of tested configurations (n = 3.2 million) remained stable for an

object size of 0% to 50% finger length in the bounded parameter search (Table 1). The simulated friction coefficient was conservative at $\mu = 0.7$.

The link length ratio was sampled from 0.68 to 1.46 which represented a 10% L_{finger} variation of the PIP joint location from the middle of the finger. This limitation was imposed as an anthropomorphic design constraint to sample joint positions near the location of the human PIP joint [19]. The entire sampled range provided stable configuration existing at varying transmission ratios, stiffness ratios and palm lengths. The mean link length ratio for a stable configuration was approximately one, inferring stable link length ratios with anthropomorphic joint positions exist. The transmission ratio was sampled from 0.01 to 1 to avoid kinematical infeasible zero distal radius $r_d = 0$ and diverging force action lines at $R_i > 1$ for grasp reliability. The stable parameter space was only 20% of the initial sample space with a mean transmission ratio of $R_i = 0.503$. A proximal tendon level arm being twice that of the distal tendon lever arm when paired with the mean link length ratio produces an equilibrium point centered in the friction cone for small angles. This alignment is intrinsically favorable for stably grasping objects that are large relative to the palm width.

The stiffness ratio was calculated from the anthropomorphic free swing trajectory and transmission ratio. Configurations with a stiffer proximal spring were preferred with a mean $K_r = 0.719$; this would decrease if a larger motion envelope ($\Delta\theta_p \gg \Delta\theta_d$) is preferred or increase if a smaller motion envelope ($\Delta\theta_p \ll \Delta\theta_d$) is preferred. Palm width normalized to finger length was sampled from 50% to ensure an object 50% of the finger length could fit within the grasp, to 150%, to ensure symmetric contact of a very small object. There was at least one stable configuration for every sampled palm width, although the transmission ratio, link length ratio and stiffness ration parameters varied. The average normalized palm width was slightly below one, however, optimal solutions discussed in the next section exist slightly higher than this average.

B. Maximizing Reliable Object Width

After stable configurations were determined for an object ranging from 0% to 50% finger length, the maximum reliable grasp span was calculated for each configuration. In Fig. 5a, the solution volume was reduced to a planar representation of varying transmission ratios (R_i). These specific ratios were chosen because most of the stable solution hull existed within the anthropomorphic constraints. The graph axis compares the link length ratio to the normalized palm width and solution spaces are graded by their respective optimal criteria or combined optimal criteria.

For the smallest listed transmission ratio $R_1 = 0.42$ the local maximum was L_{objmax}/L_{finger} = 0.946 and for the largest $R_5 = 0.42$ the local maximum was L_{objmax}/L_{finger} = 1.081. A trend of increasing max reliable object width with increasing transmission ratio was observed. The local optimum solution by transmission ratio occurred at palm widths slightly larger ($1.0 < L_{palm}/L_{finger} < 1.1$) than the
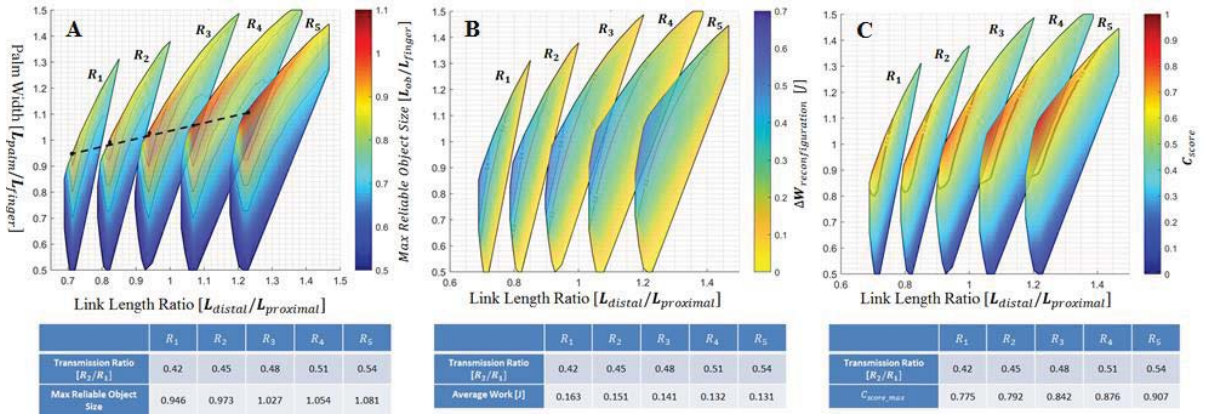
Figure 5. (A) Results of the max reliable object size segmented by transmission ratio with accompanied table displaying the max reliable object size for each transmission ratio labeled and connected by a dotted line. (B) The post-contact work for configurations contacting an object that is 50% finger length with accompanied table showing average work in each transmission ration segment. (C) The weighted score received from an optimization function weighing the post-contact reconfiguration for 0% and 50% finger length and the max reliable object size with accompanied table of max scores.

length of the finger. The global optimum $L_{objmax}/L_{finger} = 1.15$ was recorded at the largest transmission ratio $R_{objmax} = 0.583$. Without anthropomorphic sampling limitations, we would expect this value to increase as the allowable palm width and link length ratio increase. It is noted that although there is a favorable correlation for increasing palm width and link length ratio for a given transmission ratio, the local optimum of our model is located at palm lengths near the finger length. Palm designs of similar width to the finger length could be favorable for contact stability in underactuated robotic hands. It is noted that the normalization of maximum reliable object width to finger length skews the optimal solution space towards larger palms, which have a greater potential to grasp larger objects because they have a larger initial grasp span.

The approximately linear relationship between the design parameters when evaluating max stable grasp span provides a practical guideline of relative palm width, link lengths and transmission ratios for effective two-fingered precision graspers. We can conclude that the wider the range of object sizes that can be reliably grasped improves the quality of the device, especially when it comes to underactuated grippers where precision grasp is typically difficult to stabilize under arbitrary loading conditions in open loop [15].

C. Minimizing Post-Contact Work

When calculating post-contact work for the second evaluation criteria, a max actuator force of 60 N was applied, dividing 30 N to each tendon. This force represents a value near the max force production for compact highly geared DC motors commonly found in robotic hands. A reasonably strong proximal spring stiffness $K_p = 0.044 \frac{N}{m}$ was selected. The post-contact work was simulated for the same transmission ratios R_i for objects that were 0%, 25% and 50% of the finger length.

The minimum average post-contact work by transmission ratio and the global optimum post-contact work were observed for grasping the 50% finger length object. In

Fig. 5b, the local average minimum of $\Delta W = 0.131$ J was observed at R_5, this was also true for the 0% finger length configurations where minimum average $\Delta W = 0.407$ J at R_5 and at the 25% finger length configurations where minimum average $\Delta W = 0.263$ J at R_5. The transmission ratio being inversely proportional to average post-contact work was consistent across the three object widths. We believe this because a higher r_d increases the tendon force and excursion required to contact a given object, reducing the required work to reconfigure to a max actuator load. Increased performance with increased object width was also observed. Less finger motion ($\Delta\theta_p$, $\Delta\theta_d$) to contact an object produces a longer lever arm, reducing reconfiguration because force is less effectively transferred to the object from the actuation tendon. The global minimum for both the 25% and 50% graphs is essentially $\Delta W = 0$ J and is located at the maximum transmission ratio, minimum palm length and largest link length ratio. The contact line, centered in the friction cone, acts as an asymptote in which incrementally larger increases in tendon force are required for an equilibrium point to reconfigure towards this line, reducing the overall magnitude of finger reconfiguration. The low reconfiguration of these solutions indicates that the system is already near a stable position at contact where the equilibrium point is on or approaching the contact line.

The combined weighted score from the optimization function is displayed in Fig. 5c. The weighted values for this evaluation were $A_1 = 0.25$, $A_2 = 0.25$ and $A_3 = 0.50$ to equally balance max reliably object width with post-contact reconfiguration. The average C_{score} increased with increasing transmission ratio and the optimal solution was observed to be $C_{score} = 0.907$. The maximally performing 40% of stable solutions are located in the bounded lines for each transmission ratio, these values were considered for the additional stability testing.

D. Resistance to System Disturbances

Stability of the top 40% of stable solutions from the optimization function were evaluated by applying external
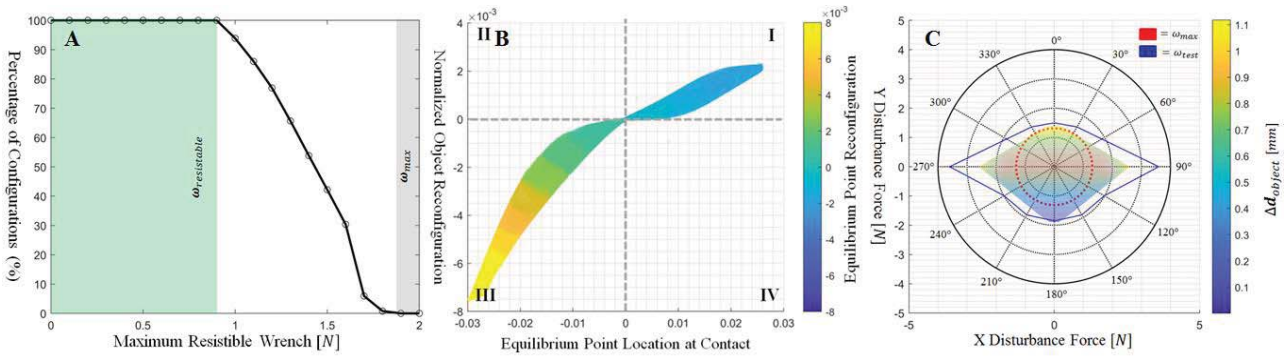
Figure 6. Three criteria were used to evaluate the stability of the top 40% of maximum performing configurations. (A) Displays the percentage of configurations that can resists a certain maximum wrench in any direction, the green section shows the wrench at which all configurations could resist and grey section describes the cutoff for maximum resistible wrench. (B) Displays the equilibrium point reconfiguration relative to object reconfiguration to show that stable solutions reconfigure towards the contact force line of action, which acts as a force asymptote. In (C) simulated and experimental external disturbance plots are compared, the simulated resistible wrench is overlaid with object motion at the force and direction.

disturbances. When evaluating these configurations, the link lengths were determined to be the anthropomorphic basis for the physical values. The finger length was set to 74mm or the size of a small female index finger [19] and the proximal tendon radius was 6mm for practical design considerations. The starting position of the configuration was the acquisition of a 37 mm object that reconfigured to an actuator load of 60 N. Each configuration was radially applied a force in 30° increments until failure criteria were reached. It was seen that all of these configurations were stable to external disturbances being able to resist a minimum of 0.98 N in all directions with the optimal configuration being able to resist 1.85 N in all directions or about 3.1% of the actuator force (Fig. 6A). A maximum resistible wrench greater than zero verifies that final stable configurations are in force closure and can resist arbitrary external wrenches. This is important to note because a significant amount of the final configurations exist on the hull of the stable solutions. Nominally the configurations were weakest in the $\pm$Y direction to force resistance and strongest in the $\pm$X direction. This is becuase the slipping failure mode was the most common and the vertical disturbance forces in the initial configuration were more likely to move the contact force F_c out of the friction cone.

In Fig. 6B, reconfiguration of the object and equilibrium point location were plotted to further understand how the system would adjust to additional actuator force. In quadrants I and III, It was seen that for all solutions the object reconfigured towards the equilibrium point. No solutions existed in quadrants II and IV which would display an object reconfiguring away from the equilibrium point with force, heading towards unstable finger poses. We can assume these configurations will remain stable with additional actuator force because the contact force line of action acts as a kinematic force asymptote and our solution space is reconfiguring towards this asymptote,.

A sample configuration in the top 40% of maximally performing solutions, parameters displayed in Table 1 and test setup in Fig. 4, was simulated and experimentally tested for external wrench resistivity (Fig. 6C). The simulation

provided stable resistance of approximately 2.5 N in the $\pm$X directions while resisting 1.3 N in the +Y and 1.9 N in the -Y directions. The minimal resistible wrench of this configuration in simulation was 1.31 N, approximately 2.2% of the actuation force. The physical test displayed an external disturbance profile similar to that of the simulation that was slightly elongated in the X directions. The gripper saw a stable resistance of approximately 3.5 N in the $\pm$X directions, 1.5 N in the +Y direction and 1.8 N in the –Y direction. The minimal resistible wrench of this configuration was 1.53 N which was similar to the 1.31 N of the simulation. Although the profile was similar, the average error between the simulated and experimental results was 22%. This can be primarily attributed to a slightly higher coefficient of friction and difficulties of visually assessing slip in the horizontal configuration where rolling instead of slipping tends to occur. When planning to manipulate an object, it is favorable to know the direction of maximum force resistance so the operator can orient the gripper such that external loading is applied in the direction of maximal disturbance resistance or so that gravity is optimally resisted.

IV. CONCLUSION

A multi-stage optimization framework was developed to evaluate the stability of symmetric two finger underactuated grippers from a single actuator in open loop force control. Anthropomorphic design parameters were sampled and key relationships between these parameters were established for the design of underactuated robotic precision graspers that can stably grasp a large variety of object sizes with minimized reconfiguration with additional grasp force. An optimal experimental design using these relationships produced a gripper was able to withstand applied object disturbances nearly five times the weight of the initial object in all directions. These relationships provide insight for the development of a variety of prosthetic hands that can successfully grasp an object in precision grasp, be proprioceptively secure and be robust to interactions with its environment. Future work includes the evaluation of higher dimensional asymmetric index-thumb precision grasping configurations using this framework.

REFERENCES

[1] C.M. Gosselin, F. Pelletier and T. Laliberté. "An Anthropomorphic Underactuated Robotic Hand with 15 Dofs and a Single Actuator." *IEEE Int. Conf. on Robotics and Automation*, California, USA, 2008.

[2] M.G. Catalano, G. Grioli, E. Farnioli, A. Serio, C. Piazza and A. Bicchi. "Adaptive synergies for the design and control of the Pisa/IIT Softhand." *The Int. Journal of Robotics Research*, Vol.33, No.5, pp.768-782, 2014.

[3] M.C. Carrozza, C. Suppo, F. Sebastiani, B. Massa, F. Vecchi, R. Lazzarini, M.R. Cutkosky and P. Dario. "The SPRING Hand: Development of a Self-Adaptive Prosthesis for Restoring Natural Grasping," *Autonomous Robots*, Vol. 16, pp. 125-141, 2004.

[4] M.T. Leddy and A.M. Dollar. "Preliminary Design and Evaluation of a Single-Actuator Anthropomorphic Prosthetic Hand with Multiple Distinct Grasp Types", *IEEE Int. Conf, on Biomedical Robotics and Biomechatronics*, Enschede, Netherlands, 2018.

[5] H. Stuart, S. Wang, O. Khatib and M. Cutkosky. "The Ocean One hands: An adaptive design for robust marine manipulation," *The Int. Journal of Robotics Research*, Vol.36, No. 2, pp.150-166, 2017.

[6] A. Rodriguez, M.T. Mason and S. Ferry. "From Caging to Grasping." *Robotics: Science and Systems*, California, USA, 2011.

[7] L. Birglen, T. Laliberté and C.M. Gosselin. *Underactuated Robotic Hands*. Springer-Verlag, 2008.

[8] A. Bicchi and V. Kumar. "Robotic Grasping and Contact: A Review." *IEEE Int. Conf. on Robotics Research and Automation*, California, USA, 2000.

[9] L. Birglen and C. Gosselin. "On the Force Capability of Underactuated Fingers." *IEEE Int. Conf. on Robotics Research and Automation*, Taipei, Taiwan, 2003.

[10] S.A. Spanjer, R. Balasubramanian, J.L. Herder and A.M. Dollar. "Improved Grasp Robustness through Variable Transmission Ratios in Underactuated Fingers." *IEEE Int. Conf. on Intelligent Robots and Systems*, Algarve, Portugal, 2012.

[11] M. Ciocarlie and P. Allen. "A constrained optimization framework for compliant underactuated grasping." *Mech. Sci.*, Vol.2, pp. 16-26, 2011.

[12] M. Haas-Heger, G. Iyengar and M. Ciocarlie. "Passive Reaction Analysis for Grasp Stability." *Trans on. Automation Science and Engineering*, Vol.15, No.3, pp.955-966, 2018.

[13] D. Prattichizzo, M. Malvezzi, M. Gabiccini and A. Bicchi. "On Motion and Force Controllability of Precision Grasps with Hands Actuated by Soft Synergies." *IEEE Trans. on Robotics*, Vol.29, No.6, pp.1440-1456, 2013.

[14] M.V. Liarokapis and A.M. Dollar. "Post-Contact, In-Hand Object Motion Compensation with Adaptive Hands." *IEEE Trans. on Automation Science and Engineering*, Vol.15, No.2, pp.456-467, 2017.

[15] L.U. Odhner, R.R. Ma and A.M. Dollar. "Open-Loop Precision Grasping With Underactuated Hands Inspired by a Human Manipulation Strategy." *IEEE Trans. on Automation and Engineering*, Vol. 10, No.3, pp.625-633, 2013.

[16] C. Ferrari and J. Canny. "Planning Optimal Grasps." *IEEE Int. Conf. on Robotics and Automation*, Nice, France, 1992.

[17] MATLAB and Parallel Computing Toolbox Release 2018a, The MathWorks, Inc., Natick, Massachusetts, Unite States.

[18] A.M. Kociolek and P.J. Keir. " Design methodology for a multifunctional hand prosthesis." *Journal of Rehabilitation Research and Development*, Vol. 32, No. 4, pp.316-324, 1995.

[19] A.R. Tilley. *The Measure of Man and Woman: Human Factors in Design,* John Wiley and Sons, New York, 2002.